

# Phase transition from Weyl to knotted semimetal using bi-circular laser

Debashree Chowdhury<sup>1,\*</sup>

<sup>1</sup>Centre for Nanotechnology, IIT Roorkee, Roorkee, Uttarakhand 247667, India

(Dated: November 20, 2024)

The Fermi surface topology of a triple non-hermitian (NH) Weyl semimetal (WSM) driven by bi-circularly polarized light is presented in this study. A NH WSM in particular has remarkable outlines. Bi-circular light, however, modifies the symmetry features of non-hermitian triple Weyl and causes an unusual new kind of band swapping. We observe swapping between the imaginary bands (with or without exceptional degeneracies), which causes unique Fermi surfaces in the form of double rings and knots. This is something never discussed before phase transition between Weyl and knotted phases. We also discuss the corresponding changes in the Berry curvature as well.

## I. INTRODUCTION

The search for new and distinct topological phases has long been at the forefront of research. Examples include the topological insulator phase (TI) [1, 2], nodal line semimetals, Dirac and Weyl-semimetal phases (WSM) [3–5], and so on. The TIs are the first instance of the materials displaying unique edge states [2], even though the majority of the sample is insulating. The other semimetallic phases mentioned here provide a three-dimensional example [4, 5]. Different properties of the 3D WSMs have been remarkably studied in the literature [3–5]. The Weyl point, also known as the source or sink of the Berry curvature, is where the two bands in WSM intersect. In this instance, the dispersion is linear, with a topological charge of  $\pm 1$ . Conversely, higher topological charge WSMs (i.e.,  $\pm 2$  or  $\pm 3$ ) are found in nature. These are the multi-WSM (double or triple WSM) [6–10]. The rotational symmetry of the point group  $C_n$  is preserved in multi-weyl having a nonlinear dispersion [11–13]. WSMs with a  $\pm 1$  charge are extensively studied, but multi-WSMs have recently gained interest. The scope to find new topological phases in this unique class of materials is thus still active. Its study must illustrate the various characteristics of hermitian and non-hermitian multi-WSMs, further driven by time-periodic fields.

The light-induced topological phases greatly aid the comprehension of topological phase transitions [14–26]. The Floquet mechanism is observed in topological materials when time-periodic fields are present. Previous research addresses light-induced topological phases when both linear and circular polarisations are present [12, 13]. Remarkably, the frequency and amplitude of the light serve as the tuning parameters for the various phases. Furthermore, the distinct Fermi surface topology—which we refer to as Lifshitz transitions—is another feature of the light-induced topological phases [27–31]. Though Floquet topological systems with circular or linear polarizations are widely addressed in the literature, bi-circular polarization-induced Floquet dynamics have just been covered in [32, 33]. "Bi-circular polarised light" refers to two superimposed circularly polarised lights with a frequency ratio of  $\eta$  merging and having a phase difference  $\alpha$ . The main

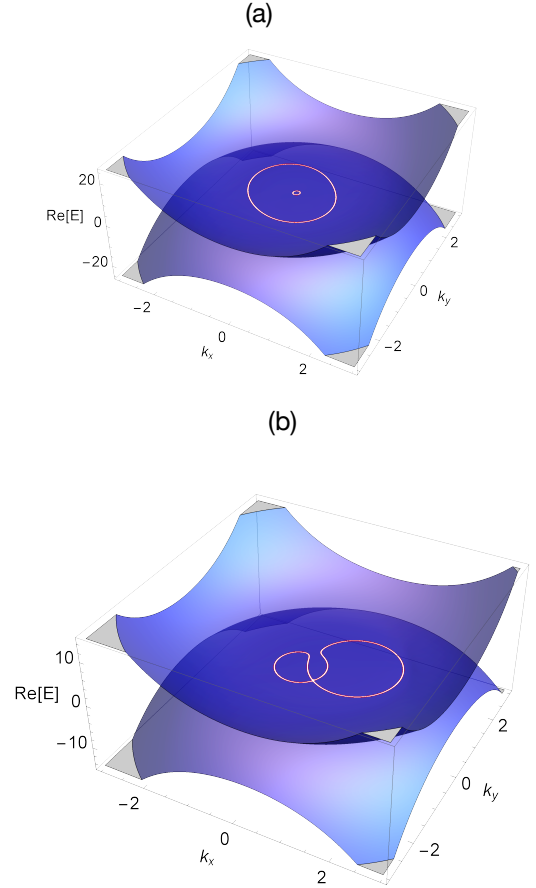


FIG. 1. Schematic for the light-induced Lifshitz transition in a triple Weyl semimetal in presence of a combination of NH terms and bi-circular polarised light. The resulting Fermi surface shows double nodal ring and knotted structures.

idea of using the bi-circular light is to have increased tunability on different topological phases. Furthermore, this unique polarization selectively breaks spatial symmetry as inversion.

On the other hand, the non-hermitian perturbation in the Hamiltonian of the WSM is interesting as long as new and fascinating topological phases are concerned [34, 35]. For the details of NH topology, the reader can go through the review

\* debashreephys@gmail.com

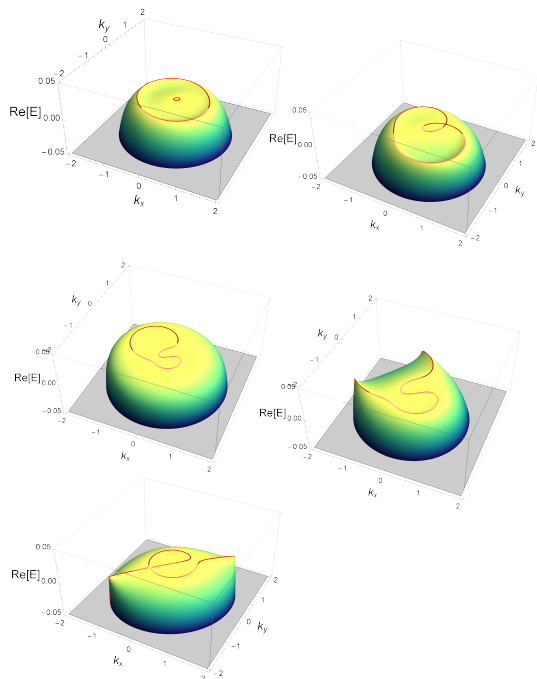


FIG. 2. The energy vs  $k_x$  and  $k_y$ , for different values of the angles  $\beta$ , keeping  $\alpha$  and  $\phi$  constant. In (a), the angle  $\beta$  is considered to be 0.1. The other angles are zero. In Fig. (b) for a slightly larger value of  $\beta = 0.2615$  the double ring structure deviates into a knotted structure. However, increasing the  $\beta$  further ( $\beta = 0.3$ ), one gets the unknotted structure as indicated in Fig. (c). For further increase of  $\beta$  produces open-ended curves indicated in figs (d), (e) and (f).

article [36]. However, the interesting issue, which makes the NH systems rich is the appearance of band swapping and as a result, the exceptional points (EP) and exceptional contours (EC) [36–43]. We summarize here a few details about the EPs, as this would help us to discuss the results. The EPs are certain special degeneracy points, where not only the eigenvalues, but eigenvectors do merge. One can show that this happens at certain positions of the band dispersion, where the real and imaginary bands cross each other. The NH double WSM are discussed in our previous papers [12, 13]. In [12, 44], it is shown that new topological phases arise in the presence of a circularly polarized light. In the NH double WSM [12] a captivating new concept of having new ECs from the parent contour is put forward. Also, the charge of the parent contour is divided into the two new ECs, with equal charges. In another paper [13], we have shown a similar system when the NH parameter has components in all three directions. This confirms that an NH hexagonally wrapped Fermi surface [45, 46] appears in the double WSM.

The present paper considers a bi-polarized light-induced NH triple WSM, and the energy dispersion shows a unique Fermi surface topology. Fig. 1 shows a glimpse of the discussed Fermi surfaces in the paper. The sequence followed in the paper is as follows. In sec. II the model Hamiltonian is discussed in the presence of the bi-circular light. This section includes our main result regarding the appearance of the dif-

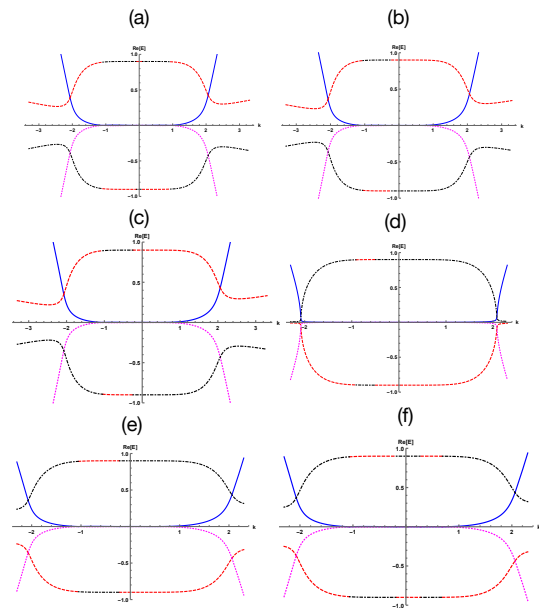


FIG. 3. 2D plot for energy vs  $k = \sqrt{k_x^2 + k_y^2}$ . In (a) the value of  $\beta = 0.1$  for this we have a mixing between imaginary bands (indicated by red and black dotted lines). However, the real and imaginary bands touch at four places, these are degenerate points but not show any exceptional behaviour. In (b) the imaginary band mixing happens in one place instead of two as is the case in plot (a). Here we choose  $\beta = 0.2615$ . Plot (c) has  $\beta = 0.3$ . Increasing values of  $\beta = 0.8$  in (d) one observes an interchange in the position of the imaginary bands. The whole story repeats for larger values of  $\beta$  in (e) and (f). But the role of the imaginary bands is reversed.

ferent nodal structures. Next in sec. III, we mainly compute the Berry curvature of the system and discuss the change in the nature of the curvature due to the change in the system parameters. We conclude in section IV.

## II. THE MODEL HAMILTONIAN

Let us start with a triple-weyl semimetal. The system Hamiltonian is given by [6, 9]

$$H(k) = v_z k_z \sigma_z + a(k_-^3 \sigma_- + k_+^3 \sigma_+), \quad (1)$$

where we denote  $k_{\pm} = k_x + ik_y$  and  $\sigma_{\pm} = \frac{1}{2}(\sigma_x + i\sigma_y)$ . The energy eigenvalues for this system are given by

$$\mathcal{E}_{\pm} = \pm \sqrt{v_z^2 k_z^2 + a^2 (k_x^2 + k_y^2)^3}. \quad (2)$$

As the next step, we would like to investigate the role of bi-circularly polarized light on the triple Weyl semimetal. Bi-circularly polarized light appears due to the superposition of two circularly polarized lights having two opposite chiralities and different frequencies of an integer multiple of  $\eta$ . The two circularly polarized lights have phase difference  $\alpha$ . The polar-

ization field induced by a bi-circularly polarized light is [32]

$$A(t) = A_0 \sqrt{2} \operatorname{Re} \left[ e^{-i(\eta\Omega t - \alpha)} \epsilon_R + e^{-i\omega t} \epsilon_L \right], \quad (3)$$

where  $A_0$  is the amplitude and  $\epsilon_{L/R}$  are left (L) and right (R) circularly polarized (CL) basis vectors. A more generic in-

cidence direction can be constructed by rotating the incident plane by an angle  $\beta$  around  $\hat{z}$ . Following [32], we write the bi-circularly polarized vector potential as

$$\begin{aligned} A_x(t) &= A_0 \left[ \cos \beta \left( \cos(\eta\Omega t - \alpha) + \cos \Omega t \right) + \sin \beta \cos \phi \left( \sin \Omega t - \sin(\eta\Omega t - \alpha) \right) \right], \\ A_y(t) &= A_0 \left[ \sin \beta \left( \cos(\eta\Omega t - \alpha) + \cos \Omega t \right) + \cos \beta \cos \phi \left( \sin \Omega t - \sin(\eta\Omega t - \alpha) \right) \right], \\ A_z(t) &= -A_0 \sin \phi \left( \sin \Omega t - \sin(\eta\Omega t - \alpha) \right), \end{aligned} \quad (4)$$

where  $\phi$  denotes the incident angle. In the presence of the gauge fields, the momentum in three directions changes as  $k_i \rightarrow k_i + \frac{eA_i}{\hbar}$ . Thus we have [12]

$$H_1 = H(k) + V(t), \quad (5)$$

where  $V(t)$  is the time-dependent part of the Hamiltonian. Using Floquet formalism in the high-frequency limit, the effective Hamiltonian is obtained as

$$H_{eff} = H(k) + \frac{1}{\hbar\Omega} [V_{-1}, V_{+1}], \quad (6)$$

where  $V_{\pm} = \int_0^T dt e^{\pm i\Omega t} V(t)$ . Here  $T = \frac{2\pi}{\Omega}$  is the time period. This is to be noted that although  $\eta$  can take any integer value, we consider  $\eta = 2$ . The effective Hamiltonian for a triple Weyl semimetal ( $n=3$ ) in the presence of bi-circularly polarized light is written as

$$\begin{aligned} H_{eff} &= (v_z k_z + i\gamma + \frac{i}{\hbar\Omega} (\mathcal{N}_1 \mathcal{N}_4 - \mathcal{N}_2 \mathcal{N}_3)) \sigma_z \\ &+ (a(k_y^3 - 3k_x^2 k_y) + \frac{i}{\hbar\Omega} (\mathcal{N}_1 + \mathcal{N}_3) \mathcal{N}_5) \sigma_y \\ &+ (a(k_x^3 - 3k_x k_y^2) - \frac{i}{\hbar\Omega} (\mathcal{N}_2 + \mathcal{N}_4) \mathcal{N}_5) \sigma_x, \end{aligned} \quad (7)$$

where  $\mathcal{N}_i$  are the function of  $k_x, k_y, \phi, \alpha, \beta$  and  $A_0$ . The exact expressions are quite cumbersome and are written in Appendix A.

$i\gamma\sigma_z$  in Eq. (7) is the non-hermitian perturbation, which makes the whole problem a non-hermitian one. This helps in understanding the non-hermitian nature of the triple Weyl semimetal in the presence of bi-circularly polarised light. The energy eigenvalues are written as,

$$\begin{aligned} \mathcal{E}_{\pm} &= \pm \frac{1}{\Omega} \left( 3a^2 k_x^4 k_y^2 \Omega^2 + 3a^2 k_x^2 k_y^4 \Omega^2 + a^2 k_x^6 \Omega^2 + a^2 k_y^6 \Omega^2 + 2N_2 (-i\Omega (ak_x^3 N_5 - 3ak_x k_y^2 N_5 + k_z N_3 v_z + i\gamma N_3) + N_1 N_3 N_4 - N_4 N_5^2) \right. \\ &- 2N_1 (-iak_y N_5 \Omega (k_y^2 - 3k_x^2) + N_4 \Omega (\gamma - ik_z v_z) + N_3 N_5^2) - 6iak_x^2 k_y N_3 N_5 \Omega - 2iak_x^3 N_4 N_5 \Omega + 6iak_x k_y^2 N_4 N_5 \Omega + 2iak_y^3 N_3 N_5 \Omega \\ &\left. - \gamma^2 \Omega^2 + k_z^2 v_z^2 \Omega^2 + 2i\gamma k_z v_z \Omega^2 - N_1^2 (N_4^2 + N_5^2) - N_2^2 (N_3^2 + N_5^2) - N_3^2 N_5^2 - N_4^2 N_5^2 \right)^{1/2}. \end{aligned} \quad (8)$$

Interestingly the results can be tuned by tuning the angles associated with the bi-circularly polarized light. We add different figures supporting different Fermi surface topologies. Let us start with the combination where all three angles are zero and we have a circular Fermi surface in the real part of the energy. We fix the two angles to zero while tuning  $\beta$ . When  $\beta = 0.1$ , one reaches the Fermi surface of a double ring structure as is indicated in Fig. 2. Increasing  $\beta$  further, at a value  $\beta = 0.2615$ , the double ring structure deviates and starts producing a nodal knot. However, for larger values of  $\beta$  the nodal knot produces an un-knotted structure. If we keep on increasing  $\beta = 0.5$ , the un-knotted closed loop deformed into an

open-ended arc. The arc is reshaped for  $\beta = 0.8$ . For  $\beta = 1.1$  we again recover the un-knotted structure. For  $\beta = 1.3$  the knotted structure is achieved again. Further increasing  $\beta$  gives the double nodal structure at  $\beta = 1.35$ . An obvious question appears what happens if we keep increasing  $\beta$  further? This repeats the whole story. Thus one may conclude that the system has a periodicity in  $\beta$ .

However, the above situation may also appear if we choose to vary  $\phi$ , keeping the other two angles at zero or properly choosing values for all the angles.

It is important to state here that the different structures, we obtain by changing the angles of the bi-circularly polarized

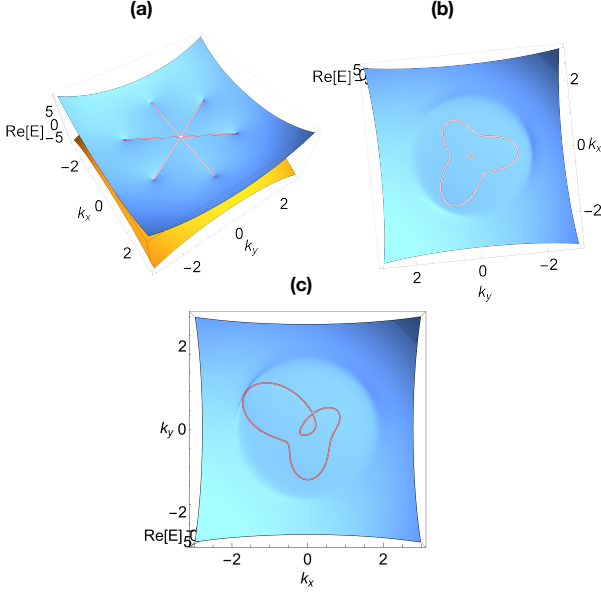


FIG. 4. 3D plot for energy vs.  $k$ . In Fig. (a) we have a hexagonally symmetric pattern for non hermitian parameter along  $\sigma_z$ , as zero and along  $\sigma_x$  is 0.1. For  $\beta = 0.1$ , keeping other angles as zero and for non hermitian parameter along  $\sigma_x$  is 0.1 and non hermitian parameter along  $\sigma_z$  is 0.9, we achieve a double nodal structure. Changing  $\beta$  to 0.2615, we achieve a knotted structure in this case as well.

light, has also a crucial dependence on the non-hermitian parameter  $\gamma$ . It then demands a discussion on whether the obtained structures are exceptional. To discuss this, we present here the 2D diagrams of  $\mathcal{E}_\pm$  vs.  $k$  in Fig. (3). Here  $k_x = k \cos(\mathcal{M})$  and  $k_y = k \sin(\mathcal{M})$ , and  $k = \sqrt{k_x^2 + k_y^2}$ . In Fig.3 (a), it is shown that when we keep the other two angles as zero and only make  $\beta = 0.1$ , the real and imaginary bands touch each other at four points, but the meeting does not take place at zero energy. Thus although the points are degenerate but not exceptional ones. Apart from that the imaginary energy bands swap between each other at two sides of the zero energy and we have a double-ring structure. Here we have a symmetric pattern. For  $\beta = 0.2615$ , although we have the same number of degenerate points, where the real and imaginary bands meet, the band swapping happens in only one place between the imaginary bands. As a result, we obtain the knotted structure. For  $\beta = 0.3$ , we get Fig. (c), which gives the unknotted closed loop. Further increase of  $\beta = 0.8$ , provides only two places, where the real and imaginary bands meet and it happens at zero energy. Thus for  $\beta = 0.8$ , we have two exceptional points. However, in this case, the imaginary bands change their positions completely and we have an open-ended arc as indicated in Fig. 3 (d). If we further increase the angle  $\beta$ , surprisingly we get the knotted structure back at  $\beta = 1.3$ . As in the previous case, the number of degenerate points is four, but the position of the imaginary bands is switched. Similarly for  $\beta = 1.35$ , we again encounter the double nodal structure, with switched imaginary bands. This shows multiple band swapping between the imaginary bands.

The above discussion considers the non-Hermitian parameter along the  $\sigma_z$  direction. However, one may also have a situation where the non-hermiticity arises in both directions of  $\sigma_x$  and  $\sigma_z$ . In the first case, when we keep non hermitian parameter along  $\sigma_z$ , to be zero and along  $\sigma_x$  is 0.1, we get a hexagonally symmetric Fermi surface for any value of  $\beta$ , with  $\alpha, \phi = 0$ . However, adding the non-hermiticity along  $\sigma_z$  as well, one can observe changes in the previous situation. For  $\beta = 0.1$ , keeping other angles as zero and for non hermitian parameter along  $\sigma_x$  is 0.1 and non hermitian parameter along  $\sigma_z$  is 0.9, we achieve a double nodal structure, but the rings are not circular rather the small one is circular but the big one is curvy. For particular values of the nonhermitian parameters in two directions and  $\beta = 0.2615$ , one achieves a knotted structure here as well. See Fig. 4 (b).

### III. THE BERRY CURVATURE

We are now in the position to discuss the topological nature of the two important structures- the double nodal ring and the knotted structure. This can be done using the Berry curvature. The left and right eigenstates of our model Hamiltonian [12, 41, 43]

$$\begin{aligned}
 \langle \psi^L | &= \left[ \left( a(k_x^3 - 3k_x k_y^2) - \frac{i}{\hbar\Omega} (\mathcal{N}_2 + \mathcal{N}_4) \mathcal{N}_5 \right) \right. \\
 &+ i \left( a(k_y^3 - 3k_x^2 k_y) + \frac{i}{\hbar\Omega} (\mathcal{N}_1 + \mathcal{N}_3) \mathcal{N}_5 \right) \\
 &\left. , \mathcal{E} - i\gamma - \left( v_z k_z + \frac{i}{\hbar\Omega} (\mathcal{N}_1 \mathcal{N}_4 - \mathcal{N}_2 \mathcal{N}_3) \right) \right] \\
 \langle \psi^R | &= \left[ \left( a(k_x^3 - 3k_x k_y^2) - \frac{i}{\hbar\Omega} (\mathcal{N}_2 + \mathcal{N}_4) \mathcal{N}_5 \right) \right. \\
 &- i \left( a(k_y^3 - 3k_x^2 k_y) + \frac{i}{\hbar\Omega} (\mathcal{N}_1 + \mathcal{N}_3) \mathcal{N}_5 \right) \\
 &\left. , \mathcal{E} - i\gamma - \left( v_z k_z + \frac{i}{\hbar\Omega} (\mathcal{N}_1 \mathcal{N}_4 - \mathcal{N}_2 \mathcal{N}_3) \right) \right]^T, \quad (9)
 \end{aligned}$$

We consider the cylindrical coordinates  $(k_\rho, \chi, k_z)$  and for that we write  $k_x = k_\rho \cos(\chi)$  and  $k_y = k_\rho \sin(\chi)$ . The Berry charge is written as,  $\mathcal{C} = \int_C \mathbf{\Omega}^{LR}(\mathbf{k}) \cdot d\mathbf{S}$ , where  $\mathbf{\Omega}^{LR}(\mathbf{k}) = \nabla \times \mathcal{A}^{LR}(\mathbf{k})$  is the Berry curvature. The superscripts on the Berry curvature denote that it is derived using the left and right eigenfunctions of the non-Hermitian Hamiltonian. Here  $\mathcal{A}^{LR}(\mathbf{k})$  is the Berry gauge field and is obtained as

$$\mathcal{A}^{LR}(k) = i \langle \psi^L(k) | \nabla | \psi^R(k) \rangle. \quad (10)$$

Next, we discuss the computed Berry curvature, which has three components  $(\Omega_{k_\rho}, \Omega_\chi, \text{ and } \Omega_{k_z})$  in cylindrical coordinates. The expressions of the three components of the Berry curvatures are cumbersome, and we do not present the explicit expressions here. However, we present plots for  $\Omega = \sqrt{\Omega_{k_\rho}^2 + \Omega_\chi^2 + \Omega_{k_z}^2}$  taking  $\alpha = \phi = 0$  and varying  $\beta$ . In Fig. 5, we have presented the results for the the two cases of double nodal ring and knotted structures. In the first case, similar to the plots in Fig. 3 (a), when  $\beta = 0.1$ , we have swapping between the imaginary band at two places and this causes divergence in the Berry curvature at two different places near

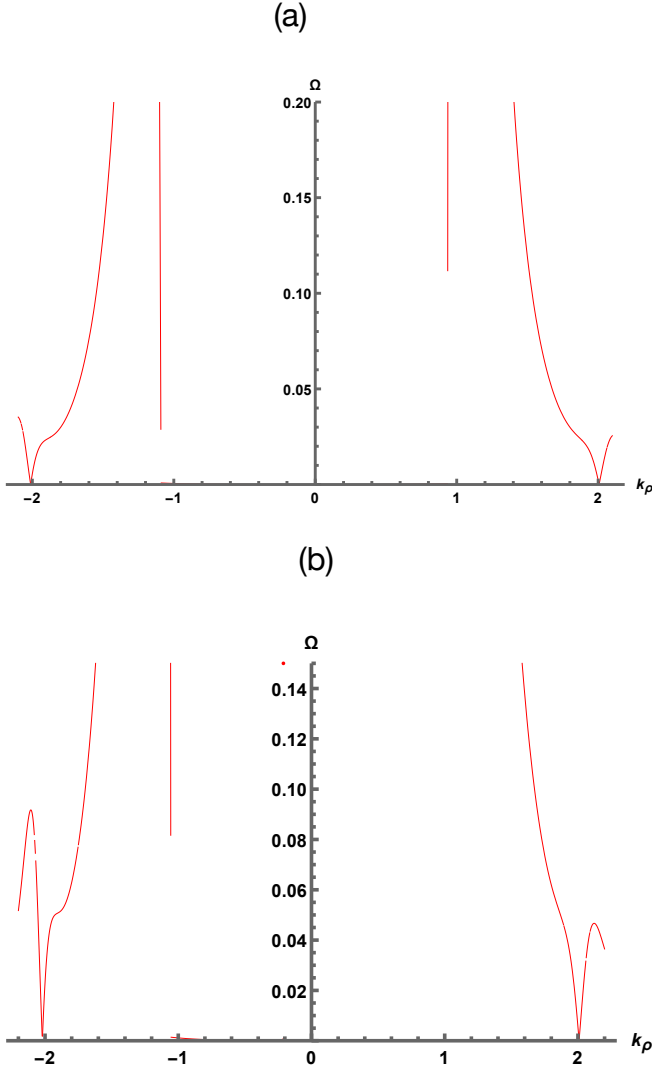


FIG. 5. Berry curvature vs  $k_\rho$  plot. In (a),  $\beta$  is chosen to be 0.1, whereas other angles are chosen to be zero. This provides a discontinuity in the plot at two places around  $k_\rho = \pm 1$ . The other discontinuity happens near  $k_\rho = \pm 2$ . In (b) ( $\beta = 0.2615$ ), the Berry curvature shows a discontinuity at  $k_\rho = -1$ . The discontinuity at  $k_\rho = \pm 2$  also appears. This resembles the 2D plots shown in Fig. 3.

the  $k_\rho = \pm 1$ . Furthermore, at  $k_\rho = \pm 2$ , we observe other divergences where the real and imaginary bands meet. The situation is presented in Fig. 5 (a). In Fig. 5 (b), the Berry curvature for  $\beta = 0.2615$  is plotted and the situation shows divergence only at  $k_\rho = -1$ . The other divergences occur at  $k_\rho = \pm 2$ .

#### IV. CONCLUSION

In this paper, we have analysed a dissipated (gain/loss) triple WSM in the presence of a bi-circularly polarized light. The magic of this particular polarization is that it provides better tunability by providing three tuning parameter angles. This kind of light provides spatial symmetry breaking in the crystal and is thus responsible for unique topological phases. The system we choose is the triple WSM, which has a  $C_6$  rotational symmetry having a non-linear dispersion. However, once the bi-circular light is switched on, the light breaks spatial inversion and in a combined effect of non-hermiticity and the light, we eventually land up in a double nodal ring and knotted semimetals. This is the novelty of this work. Thus the bi-circular light can be thought of as an important tool to switch between triple WSM to different nodal structures. We have also discussed the topological nature of the structures by analysing the Berry curvature.

*Acknowledgments:* D.C. acknowledges financial support from DST (project number DST/WISE-PDF/PM-40/2023). D.C would also like to thank Dr. Awadhesh Narayan for several discussions.

#### Appendix A: The effective Hamiltonian and its components

The effective Hamiltonian after the Floquet high frequency approximation

$$\begin{aligned}
 H_{eff} = & v_z k_z \sigma_z + a(k_-^3 \sigma_- + k_+^3 \sigma_+) + \frac{i}{\hbar\Omega} (N_1 N_4 - N_2 N_3) \sigma_z + \frac{i}{\hbar\Omega} (N_1 + N_3) N_5 \sigma_y \\
 & - \frac{i}{\hbar\Omega} (N_2 + N_4) N_5 \sigma_x,
 \end{aligned} \tag{A1}$$

where

$$N_1 = \frac{1}{32} A_0 (36aA_0^2 \cos^3(\beta) - 27aA_0^2 \cos(\beta) + 27aA_0^2 \cos(3\beta) + 2 \cos(\beta) (-3a(3A_0^2 - 8k_x^2 + 8k_y^2)$$

$$\begin{aligned}
& + 9aA_0 \left( A_0 \sin^2(\phi) + 4ik_y \sin(\alpha) \sin(\beta) \right) - 3aA_0 \cos^2(\phi) (3A_0 + 8ik_y \sin(\alpha) \sin(\beta)) + 48iak_x k_y \cos(\phi) \\
& + \frac{1}{2} i \left( 3 \sin(\beta) \left( 9aA_0^2 \cos(2\beta) \cos(\phi) - 6aA_0^2 \sin^2(\beta) \cos(3\phi) + 15aA_0^2 \cos(\phi) - 32ak_x^2 \cos(\phi) + 64iak_x k_y + 32ak_y^2 \cos(\phi) \right) \right. \\
& + 8A_0 \sin(\alpha) (-3ak_x \cos(2\beta) (\cos(2\phi) + 3) + \cos(2\phi) (3ak_x - 3ak_y \sin(2\beta))) + 9ak_x + 24iak_y \cos(\phi) \left. \right) \\
& + 3aA_0 \cos^2(\beta) \left( 36iA_0 \sin(\beta) \cos^3(\phi) - 8ik_x \sin(\alpha) (\cos(2\phi) + 3) \right) \\
& + 8A_0 \cos(\alpha) \left( 3ak_x \cos(2\beta) (\cos(2\phi) + 3) - 6ak_y \sin(2\beta) \sin^2(\phi) - 12iak_y \cos(\phi) \right), \\
\mathcal{N}_2 = & \frac{1}{32} A_0 \left( -36iaA_0^2 \cos^3(\beta) \cos^3(\phi) + 12i \cos(\beta) \left( 9aA_0^2 \sin^2(\beta) \cos^3(\phi) + 3aA_0^2 \cos(\phi) - 4aA_0 k_x \sin(\alpha) \sin(\beta) \cos^2(\phi) \right) \right. \\
& + 6aA_0 k_x \sin(\alpha) \sin(\beta) + 4ak_x^2 \cos(\phi) + 8iak_x k_y - 4ak_y^2 \cos(\phi) \left. \right) + \frac{1}{2} i \left( \sin(\beta) \left( 36iaA_0^2 \cos(2\beta) + 4i \left( 9aA_0^2 \cos(2\phi) + 24ak_x^2 - 24ak_y^2 \right) \right) \right. \\
& + 192ak_x k_y \cos(\phi) \left. \right) + 8A_0 \sin(\alpha) (-3 \cos(2\phi) (ak_x \sin(2\beta) + ak_y) + 24iak_x \cos(\phi) + 3ak_y \cos(2\beta) (\cos(2\phi) + 3) - 9ak_y) \\
& + 8A_0 \cos(\alpha) \left( -6ak_x \sin(2\beta) \sin^2(\phi) - 12iak_x \cos(\phi) - 3ak_y \cos(2\beta) (\cos(2\phi) + 3) \right) \\
& + 3aA_0 \cos^2(\beta) (-36A_0 \sin(\beta) + 8ik_y \sin(\alpha) (\cos(2\phi) + 3)), \\
\mathcal{N}_3 = & \frac{1}{32} A_0 \left( -9iaA_0^2 \sin(3\beta) \cos^3(\phi) + 36aA_0^2 \cos^3(\beta) - 27aA_0^2 \cos(\beta) + 27aA_0^2 \cos(3\beta) \right. \\
& + \cos(\beta) \left( -18aA_0^2 \cos^2(\phi) - 9aA_0^2 + 3aA_0 \left( -3A_0 \cos(2\phi) - 32ik_y \sin(\alpha) \sin(\beta) \sin^2(\phi) \right) + 48a \left( k_x^2 - k_y^2 \right) - 96iak_x k_y \cos(\phi) \right) \\
& + \frac{1}{4} \sin(\beta) \left( -i \cos(\phi) \left( 63aA_0^2 + 192a \left( k_y^2 - k_x^2 \right) \right) + 27iaA_0^2 \cos(3\phi) - 384ak_x k_y \right) \\
& + 3aA_0 \cos^2(\beta) \left( 8ik_x \sin(\alpha) (\cos(2\phi) + 3) - 36iA_0 \sin(\beta) \cos^3(\phi) \right) + 12iaA_0 k_x \sin(\alpha) \cos(2\beta) (\cos(2\phi) + 3) \\
& + 8A_0 \cos(\alpha) \left( 3ak_x \cos(2\beta) (\cos(2\phi) + 3) - 6ak_y \sin(2\beta) \sin^2(\phi) + 12iak_y \cos(\phi) \right) - 12iA_0 \sin(\alpha) (ak_x \cos(2\phi) + 3ak_x - 8iak_y \cos(\phi)), \\
\mathcal{N}_4 = & \frac{1}{32} A_0 \left( 36iaA_0^2 \cos^3(\beta) \cos^3(\phi) - 9aA_0^2 \sin(3\beta) + \cos(\beta) \left( -108iaA_0^2 \sin^2(\beta) \cos^3(\phi) - 4i \cos(\phi) \left( 9aA_0^2 + 12ak_x^2 - 12ak_y^2 \right) \right) \right. \\
& - 96iaA_0 k_x \sin(\alpha) \sin(\beta) \sin^2(\phi) - 96ak_x k_y \left. \right) + \sin(\beta) \left( -18aA_0^2 \cos(2\phi) + 9aA_0^2 - 48ak_x^2 - 96iak_x k_y \cos(\phi) + 48ak_y^2 \right) + 8A_0 \cos(\alpha) \\
& \left( -6ak_x \sin(2\beta) \sin^2(\phi) + 12iak_x \cos(\phi) - 3ak_y \cos(2\beta) (\cos(2\phi) + 3) \right) + 12iA_0 \sin(\alpha) (8iak_x \cos(\phi) + ak_y \cos(2\phi) + 3ak_y) \\
& + 3aA_0 \cos^2(\beta) (-36A_0 \sin(\beta) - 8ik_y \sin(\alpha) (\cos(2\phi) + 3)) - 12iaA_0 k_y \sin(\alpha) \cos(2\beta) (\cos(2\phi) + 3), \\
\mathcal{N}_5 = & \frac{1}{2} iA_0 v_z \sin(\phi). \tag{A2}
\end{aligned}$$

- 
- [1] M. Z. Hasan and C. L. Kane, *Rev. Mod. Phys.* **82**, 3045 (2010).  
[2] C. L. Kane and E. J. Mele, *Phys. Rev. Lett.* **95**, 226801 (2005).  
[3] O. Vafek and A. Vishwanath, *Annu. Rev. Condens. Matter Phys.* **5**, 83 (2014).  
[4] A. A. Burkov, *Nature Materials* **15**, 1145 (2016).  
[5] N. P. Armitage, E. J. Mele, and A. Vishwanath, *Rev. Mod. Phys.* **90**, 015001 (2018).  
[6] Amit Gupta, arXiv:1703.07271.  
[7] Shin-Ming Huang et al, *PNAS*, **113**, 1180, (2016).  
[8] C. Fang, M. J. Gilbert, X. Dai, and B. Andrei Bernevig, *PRL* **108**, 266802 (2012).  
[9] Shi-Xin Zhang, Shao-Kai Jian, and Hong Yao, *Phys. Rev. B* **96**, 241111(R) (2017).  
[10] Chen Fang, Matthew J. Gilbert, Xi Dai, and B. Andrei Bernevig, *Phys. Rev. Lett.* **108**, 266802 (2012).  
[11] Shin-Ming Huang et. al., *PNAS*, **113** (5), 1180 (2016).  
[12] D. Chowdhury, A. Banerjee, and A. Narayan, *Phys. Rev. A* **103**, L051101, (2021).  
[13] Debashree Chowdhury, Ayan Banerjee, and Awadhesh Narayan *Phys. Rev. B* **105**, 075133, (2022).  
[14] T. Oka and H. Aoki, *Phys. Rev. B* **79**, 081406(R) (2009).  
[15] J. Cayssol, B. Dóra, F. Simon, and R. Moessner, *Phys. Status Solidi RRL* **7**, 101 (2013).  
[16] N. H. Lindner, G. Refael, and V. Galitski, *Nat. Phys.* **7**, 490 (2011).  
[17] M. C. Rechtsman, J. M. Zeuner, Y. Plotnik, Y. Lumer, D. Podolsky, F. Dreisow, S. Nolte, M. Segev, and A. Szameit, *Nature (London)* **496**, 196 (2013).  
[18] Y. Wang, H. Steinberg, P. Jarillo-Herrero, and N. Gedik, *Science*, **342**, 453 (2013).  
[19] M. S. Rudner and N. H. Lindner, arXiv:2003.08252.  
[20] A. Narayan, *Phys. Rev. B* **91**, 205445 (2015).  
[21] Z. Yan and Z. Wang, *Phys. Rev. Lett.* **117**, 087402 (2016).  
[22] C. K. Chan *et al.*, *Phys. Rev. B* **94**, 121106 (2016).

- [23] A. Narayan, Phys. Rev. B **94**, 041409(R) (2016).
- [24] K. Taguchi, D. Xu, A. Yamakage, and K. T. Law, Phys. Rev. B **94**, 155206 (2016).
- [25] Z. Yan and Z. Wang, Phys. Rev. B **96**, 041206(R) (2017).
- [26] R. Jaiswal and A. Narayan, Phys. Rev. B **102**, 245416 (2020).
- [27] J. W. McIver, B. Schulte, F.-U. Stein, T. Matsuyama, G. Jotzu, G. Meier and A. Cavalleri Nature Physics **16**, 38(2020).
- [28] S. A. Sato, J. W. McIver, M. Nuske, P. Tang, G. Jotzu, B. Schulte, H. Hübener, U. De Giovannini, L. Mathey, M. A. Sentef, A. Cavalleri, and A. Rubio, Phys. Rev. B **99**, 214302(2019).
- [29] Hannes Hübener, Michael A. Sentef, Umberto De Giovannini, Alexander F. Kemper and Angel Rubio, Nature Communications, **8**, 13940 (2017).
- [30] Edbert Sie et al. Nature **565**, 61(2019).
- [31] Robert J. Kirby et al. arXiv:2011.04646.
- [32] Thaís V. Trevisan , Pablo Villar Arribi , Olle Heinonen , Robert-Jan Slager , and Peter P. Orth, Phys. Rev. Lett. **128**, 066602 (2022).
- [33] T. Nag, R.-J. Slager, T. Higuchi, and T. Oka, Phys. Rev. B **100**, 134301 (2019).
- [34] Luis E F Foa Torres, Journal of Physics: Materials, **3**, 1 (2019).
- [35] V. M. Alvarez, J. B. Vargas, M. Berdakin, and L. F. Torres, Eur. Phys. J.: Spec. Top. **227**, 1295 (2018).
- [36] E. J. Bergholtz, J. C. Budich, and F. K. Kunst, Rev. Mod. Phys. **93**, 15005 (2021).
- [37] S. Jana, D. Chowdhury, A. Saha, arXiv:2010.02852.
- [38] A. Ghatak and T. Das, J. Phys.: Condens. Matter **31**, 263001 (2019).
- [39] Z. Gong, Y. Ashida, K. Kawabata, K. Takasan, S. Higashikawa, and M. Ueda, Phys. Rev. X **8**, 031079 (2018).
- [40] A. Banerjee and A. Narayan, J. Phys.: Condens. Matter **33**, 225401, (2021).
- [41] A. Cerjan, M. Xiao, L. Yuan, and S. Fan, Phys. Rev. B **97**, 075128 (2018).
- [42] C. Yin, H. Jiang, L. Li, R. Lü, and S. Chen, Phys. Rev. A **97**, 052115, (2018).
- [43] A. Cerjan, S. Huang, M. Wang, K. P. Chen, Y. Chong and M. C. Rechtsman, Nature Photonics,**13**, 623 (2019).
- [44] A. Banerjee and A. Narayan, Phys. Rev. B **102**, 205423 (2020).
- [45] L. Fu, Phys. Rev. Lett. **103**, 266801 (2009).
- [46] S. Basak, H. Lin, L. A. Wray, S.-Y. Xu, L. Fu, M. Z. Hasan, and A. Bansil, Phys. Rev. B **84**, 121401(R), (2011).